Response of a vertical natural convection boundary layer to random and single-mode perturbations

Yongling Zhao, Chengwang Lei and John C. Patterson

School of Civil Engineering
The University of Sydney, Sydney, NSW 2006, Australia

Abstract

A direct stability analysis is conducted to investigate the convective instabilities of a natural convection boundary layer adjacent to an isothermally heated plate at $Ra = 4.5 \times 10^9$ and $Pr = 7.0$. A previously reported frequency-filtering effect of the thermal boundary layer is clearly demonstrated by a random perturbation experiment. It is found that the entire thermal boundary layer may be divided into three regions according to the frequency evolution, which include an upstream low-frequency region, a transitional region (with both low and high frequency bands) and a downstream high-frequency region. The thermal boundary layer may also be divided into two distinct sections based on the power of its spectral response, i.e. an upstream damping section with decaying power and a downstream amplifying section with increasing power. Furthermore, single-mode perturbation experiments have been conducted to demonstrate the occurrence of resonance in the thermal boundary layer. It is found that the resonance can be triggered over a particular band of frequencies, which is referred to as the frequency band of resonance.

Introduction

Stability characteristics of natural convection boundary layer flows are of continuing research interest because of its importance to the understanding of laminar-turbulent transition which in turn determines the rate of heat transfer.

Previous stability analysis and experimental results show that a vertical natural convection boundary layer sharply filters random propagating perturbations to a dominant frequency and favours a certain band of disturbance frequencies for amplification. One of the pioneering experimental studies was performed by Eckert and Soehnghen [1], in which a Mach Zehnder interferometer was used to observe a laminar boundary layer flow in air subjected to natural disturbances. The experiments demonstrated that the boundary layer amplified a certain range of disturbance frequencies. Subsequent experiments by Hollman et al. [2] and Polymeropoulos and Gebhart [3] found similar behaviour.

Theoretical study for predicting the frequency filtering behaviour of a vertical natural convection boundary layer subjected to uniform heat flux was firstly conducted by Dring and Gebhart [4]. A further study by Gebhart and Mahajan [5] concluded that the characteristic frequency of a vertical natural convection boundary layer flow only depends on the heating condition and the fluid properties. A good review of the theoretical and experimental studies concerning instabilities of a vertical boundary layer is available in Gebhart [6].

The present direct stability analysis is to further reveal the frequency-filtering effect in detail. Furthermore, numerical evidence for the occurrence of resonance in the thermal boundary layer is presented and discussed.

Problem Formulation and Numerical Method

The flow of interest is a two-dimensional natural convection boundary layer flow of a Newtonian fluid ($Pr = 7$) formed adjacent to an isothermally heated vertical surface (refer to the schematic shown in figure 1). The height of the heated plate is H and the width of the computational domain is of $L_e = 0.5H$, which is determined based on the scale of the thickness of the viscous boundary layer (Patterson and Imberger [7]) to ensure that the right boundary is located sufficiently far from the outer edge of the viscous boundary layer. To minimize the effects of the lower horizontal boundary on the numerical solution, the plate is extended downwards by H_e. The same strategy was adopted in Lin et al. [8].
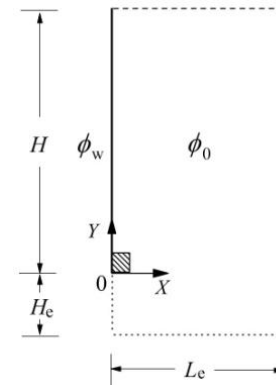

Figure 1. Schematic of the computational domain, with the shaded square near the leading edge of the heated surface showing the location of the superimposed perturbation source. Here ϕ_0 is the ambient fluid temperature and ϕ_w is the temperature of the heated surface at $t \geq 0$.

The fluid in the considered domain initially is stationary and isothermal at the temperature ϕ_0. The temperature of the rigid surface of interest is instantaneously raised to and maintained at ϕ_w at the start-up. The boundary conditions for the two boundaries of the extended region are rigid non-slip and adiabatic. The top and right far field boundaries are open boundary conditions where any backflow from the exterior is considered to be at the reference temperature ϕ_0.

The flow in the considered domain is described by the two-dimensional Navier–Stokes and energy equations. The non-dimensional form of these governing equations, under the Boussinesq approximation, can be expressed as follows:

$$\frac{\partial u}{\partial x}+\frac{\partial v}{\partial y}=0 \qquad (1)$$

$$\frac{\partial u}{\partial t}+u\frac{\partial u}{\partial x}+v\frac{\partial u}{\partial y}=-\frac{\partial p}{\partial x}+(\frac{\partial^2 u}{\partial x^2}+\frac{\partial^2 u}{\partial y^2}) \qquad (2)$$

$$\frac{\partial v}{\partial t}+u\frac{\partial v}{\partial x}+v\frac{\partial v}{\partial y}=-\frac{\partial p}{\partial y}+(\frac{\partial^2 v}{\partial x^2}+\frac{\partial^2 v}{\partial y^2})+\frac{Ra}{Pr}T \qquad (3)$$

$$\frac{\partial T}{\partial t}+u\frac{\partial T}{\partial x}+v\frac{\partial T}{\partial y}=\frac{1}{Pr}(\frac{\partial^2 T}{\partial x^2}+\frac{\partial^2 T}{\partial y^2})+S \qquad (4)$$

where u and v are the velocity components in x and y directions respectively, p is the pressure, t is the time, T is the temperature. The quantities u, v, x, y, p, t and T are the corresponding dimensionless forms of U, V, X, Y, P, τ and ϕ, which are normalized as $u=\frac{U}{\nu H^{-1}}$, $v=\frac{V}{\nu H^{-1}}$, $x=\frac{X}{H}$, $y=\frac{Y}{H}$, $t=\frac{\tau}{H^2\nu^{-1}}$, $p=\frac{P}{\rho\nu^2 H^{-2}}$ and $T=\frac{\phi-\phi_0}{\phi_w-\phi_0}$. Here ρ and ν is the density and kinematic viscosity of the fluid at the reference ambient temperature ϕ_0 and ϕ_w is the temperature of the heated surface. The Rayleigh and Prandtl numbers are defined as:

$$Ra=\frac{g\beta\Delta\phi H^3}{\nu\kappa}, \; Pr=\frac{\nu}{\kappa} \qquad (5)$$

where g is the gravitational acceleration, κ and β are the thermal diffusivity and thermal expansion coefficient of working fluid (water) at the reference ambient temperature ϕ_0. Quantity $\Delta\phi=\phi_w-\phi_0$ is the temperature difference between the heated plate and the ambient.

A single value of Ra and Pr are considered here; $Ra=4.5\times10^9$, $Pr=7.0$. The results for a wider range of these parameters will be reported separately.

The term S in the energy equation is used to introduce artificial perturbations in a small region ($0\le x\le0.02$ and $0\le y\le0.02$) at the base of the thermal boundary layer, as shown in figure 1. Two types of perturbations, a random-mode and a single-mode, are investigated here. For the random perturbation experiments, the source term S is specified as $S=2A\cdot(rand(t)-0.5)$ with $A=9$. Here $rand(t)$ is a random number generator, generating numbers between 0 and 1; and A is the perturbation amplitude which is determined according to the amplitude adopted in Armfield and Janssen [9]. As the thermal boundary layer flow considered in Armfield and Janssen [9] is in the context of an internal flow in an enclosed cavity, which is different from the present investigation in which the flow is external and there is no thermal stratification, further numerical tests have been conducted to ensure the response of the thermal boundary layer to the perturbations is linear. For the single-mode perturbation experiments, the source term is specified as $S=A_s\cdot\sin(2\pi f_{pt}t)$.

Here f_{pt} is the perturbation frequency and A_s is the perturbation amplitude which is chosen to be $3.6A$ so that spatial amplification characteristics can be discerned clearly at the Rayleigh number $Ra=4.5\times10^9$ considered in the present study.

The governing equations along with the initial and boundary conditions are solved implicitly using a finite-volume method with the SIMPLE scheme (Patankar [10]) for pressure-velocity coupling. The spatial derivatives are discretized using the second-order central-differencing scheme except for the advection terms

which are approximated by the QUICK scheme (see Leonard [11]). The unsteady terms are integrated by a second order backward difference scheme. Mesh and time-step dependency tests have been conducted with three mesh systems ($400\times149, 700\times249$ and 800×299) and three time-steps ($\Delta t=1.7\times10^{-7}, 1/2\Delta t$ and $4\Delta t$). Based on these tests, the mesh system 700×249 and the time-step $\Delta t=1.7\times10^{-7}$ are adopted.

Results and Discussion

Response to Random Perturbations

In order to obtain insights into the frequency-filtering effect and frequency evolution behaviour of the thermal boundary layer, a direct stability analysis is performed, with random perturbations superimposed onto the base flow at the upstream of the boundary layer.
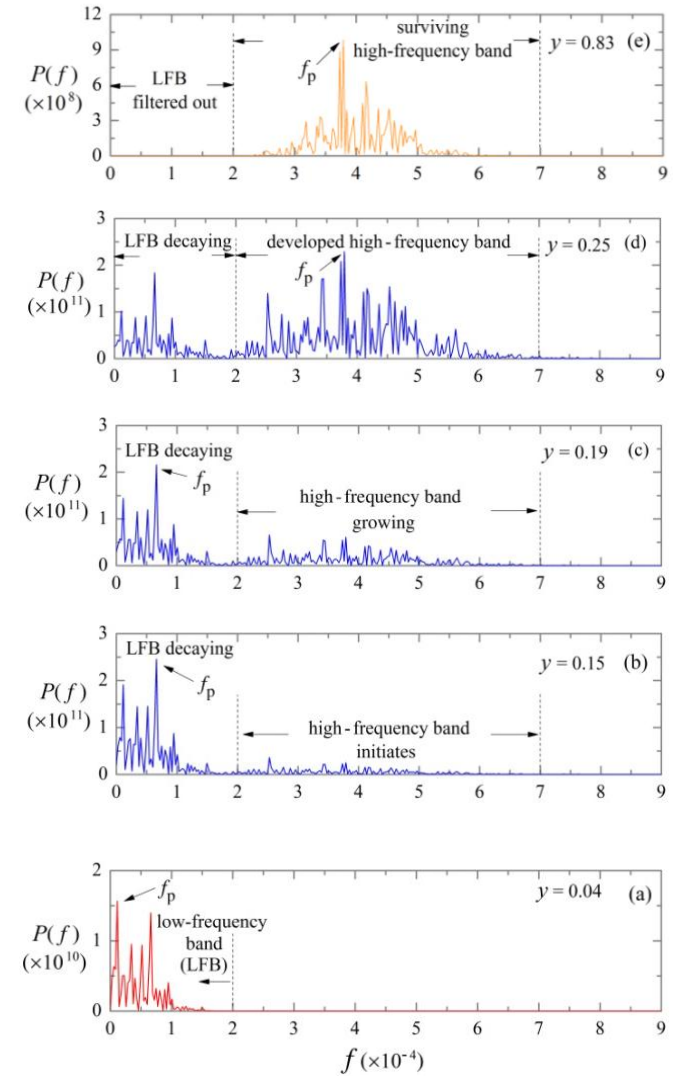

Figure 2. Power spectra of the temperature time series at various stream-wise locations, demonstrating the evolution of the boundary layer frequencies. (a) the upstream low-frequency region; (b), (c) and (d) the transitional region with both the low and high-frequency bands; (e) the downstream high-frequency region.

Spectral analyses of the temperature time series (obtained at $x=6.25\times10^{-3}$) at the quasi-steady stage are carried out to examine the frequency-filtering effect of the thermal boundary layer. Figure 2 presents the spatial evolution of the spectra of the temperature time series in the stream-wise direction (from bottom

to top). It is clear in figure 2 that the boundary layer may be divided into three distinct regions, which includes an upstream low-frequency region, a transitional region (with both low and high frequencies) and a downstream high-frequency region. It is worth noting that the random perturbations introduced upstream are similar to white noise which contains a full range of frequencies. It is seen in figure 2(a) that only a narrow band of low frequencies of the random perturbations has survived in the upstream boundary layer. As the perturbations are convected downstream, another high-frequency band appears in the spectra and grows as it travels in the stream-wise direction while in the meantime the low-frequency band decays (indicated by the variation of the power of the two bands shown in figures 2(b), (c) and (d) respectively). This intermediate region with the co-existence of both the low and high-frequency bands can be referred to as the transitional region. Further downstream, as shown in figure 2(e), the low-frequency band has been completely filtered out by the boundary layer, whereas the high-frequency band has survived. This high-frequency band can be referred to as the characteristic frequency band of the thermal boundary layer as it determines the instability and resonance properties of the thermal boundary layer. These properties will be revealed by the single-mode perturbation experiments to be described in the following section. Note that here the dividing frequencies of the low and high frequency bands of the boundary layer shown in figure 2 are indicative only. The lower and upper bounds of the frequency band are approximately determined in the following section.
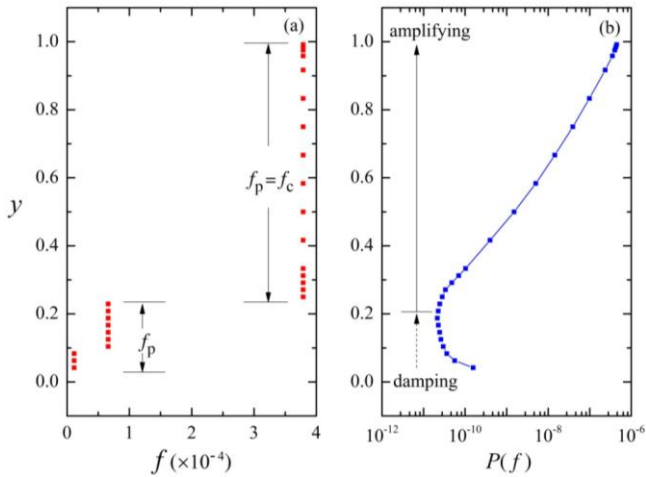

Figure 3. Spatial evolution of the peak frequency and the corresponding power. (a) peak frequency and (b) spectral power at the peak frequency.

The peak frequencies (with the highest power on the spectra) at different stream-wise locations of the boundary layer are also indicated in figure 2. It is seen in figures 2(a)-(c) that in the upstream part of the boundary layer, the peak frequency initially appears in the low-frequency band. Further downstream, associated with the decay of the low-frequency band and the growth of the high-frequency band, the peak frequency shifts to the high-frequency band (i.e. the characteristic frequency band of the thermal boundary layer), as shown in figures 2(d) and (e). It is also observed that above the height $y = 0.25$ the peak frequency remains unchanged, which is therefore referred to as the characteristic frequency of the thermal boundary layer (refer to Gebhart and Mahajan [5]). The spatial evolution of the peak frequency f_p and its corresponding power $P(f)$ in the stream-wise direction are plotted in figure 3. It is interesting to note that the evolution of the peak frequency appears as a three-step development, approximately corresponding to the three distinct

regions described above. Figure 3(a) confirms that the characteristic frequency appears around $y = 0.25$, and beyond this location the peak frequency remains unchanged. The dimensionless characteristic frequency determined by this random perturbation experiments is approximately 37900 for the present case. It is also seen in figure 3(b) that the spatial evolution of the spectral power of the peak frequency includes two stages, firstly a decaying stage upstream and secondly an amplifying stage downstream. The decaying stage is constrained in a small upstream region, which covers the low-frequency region and most of the transitional region described above.

Response to Single-mode Perturbations

The response of the thermal boundary layer to single-mode perturbations of different perturbation frequencies is demonstrated in figure 4. The temperature time series in this figure are all obtained at $y = 0.83$. It is seen that the maximum oscillation amplitude at the quasi-steady stage is triggered by the perturbation at the characteristic frequency f_c. As the perturbation frequency deviates from the characteristic frequency in either direction, the amplitude of the temperature response decreases. This result clearly demonstrates that the thermal boundary layer only responds to a particular band of frequencies which may be referred to as the frequency band of resonance B_r.
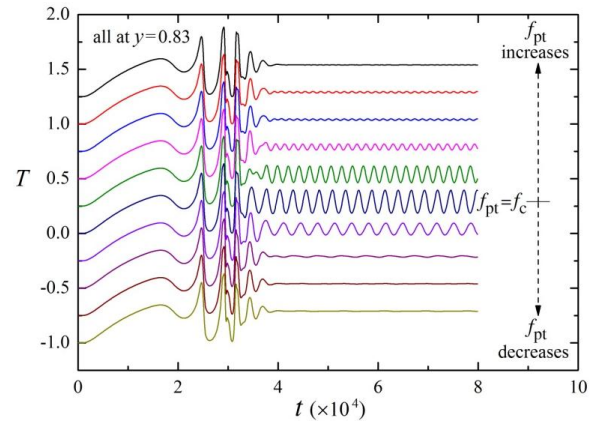

Figure 4. Temperature time series at $y = 0.83$ in the thermal boundary layer perturbed at different perturbation frequencies. The interval of two consecutive perturbation frequencies is 8600. The temperature time series are shifted vertically for clarity. The shifted values can be seen from the temperature at $t = 0$.

The stream-wise temperature profiles at $t = 6 \times 10^{-4}$ (i.e. in the quasi-steady stage, refer to figure 4) in the thermal boundary layers perturbed at different perturbation frequencies are shown in figure 5, in which the temperature is measured along the vertical line of $x = 6.25 \times 10^{-3}$ and the interval of the perturbation frequency Δf is of 8600. Figure 5 shows that the perturbation at the characteristic frequency results in the largest wave amplitude in the downstream boundary layer, whereas perturbations at frequencies deviated from the characteristic frequency results in much smaller wave amplitudes. The temperature fluctuation becomes negligibly small at $f_{pt} = f_c + 3\Delta f$ and $f_{pt} = f_c - 3\Delta f$, suggesting that the boundary layer responds to a frequency band approximately between $f_c - 3\Delta f \sim f_c + 3\Delta f$. It is also seen that the oscillations of the temperatures are indiscernible in the upstream part of the boundary layer. However, the perturbations start to grow above a certain height and are amplified rapidly in the stream-wise direction.
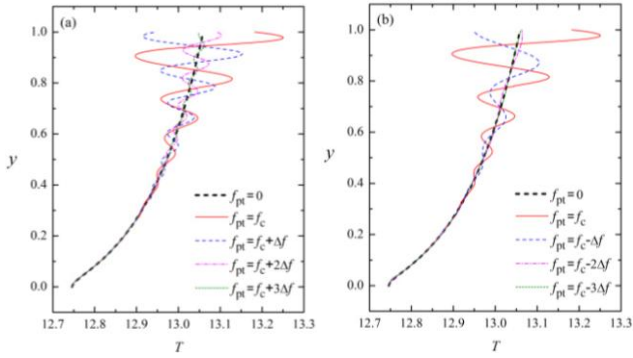
Figure 5. The stream-wise temperature profiles along $x = 6.25 \times 10^{-3}$ in the thermal boundary layer at $t = 6 \times 10^{-4}$. (a) Profiles in the boundary layers perturbed at $f_{pt} \geq f_c$; and (b) profiles in the boundary layer perturbed at $f_{pt} \leq f_c$. The interval Δf is 8600 and $f_{pt} = 0$ represents the unperturbed case.

The numerical evidence presented above has clearly demonstrated that the thermal boundary layer favours a particular band of perturbation frequencies for amplification. The lower and upper bounds of the frequency band is approximately determined below.
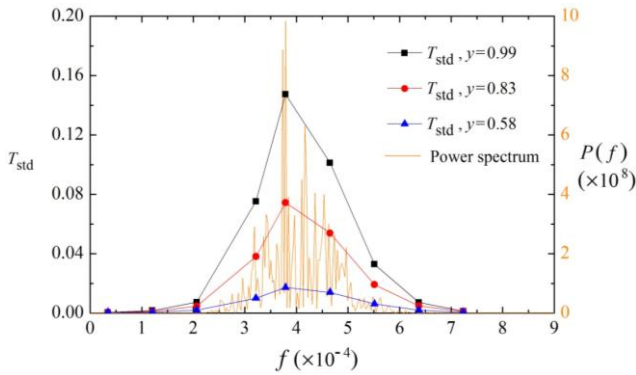

Figure 6. Comparison of the frequency bands obtained from the random and single-mode perturbation experiments.

Figure 6 plots the standard deviation of the temperature oscillations against the frequency of the single-mode perturbations at three different locations. The power spectrum of the temperature time series obtained at $y = 0.83$ in the random perturbation experiment is also superimposed on the plot. As expected, the maximum standard deviation is observed at all three locations at a perturbation frequency around 38000, which is approximately the same as the characteristic frequency of the thermal boundary layer identified above. Figure 6 also shows excellent correlation between the random-mode perturbation and single-mode perturbation experiments in terms of the frequency response. Both numerical experiments suggest that the lower bound f_{LB} of the characteristic frequency band is about 2×10^4 and the upper frequency bound f_{UB} is approximately at 7×10^4. This result implies that the resonance frequency band of a thermal boundary layer at a given Rayleigh number can be determined by performing either random or single-mode perturbation experiment. In fact, the characteristic frequency band of the thermal boundary layer (i.e. the survived high-frequency band shown in figure 2(e)) determines the resonance properties of the thermal boundary layer.

Conclusions

Direct stability analysis has been used to investigate the instability and resonance characteristics of the natural convection boundary layer formed adjacent to an isothermally heated vertical flat plate.

The spatial evolution of the boundary layer frequencies is visualized from the spectra of the temperature time series in the stream-wise direction. It is found that the thermal boundary layer exhibits three distinct frequency regions, i.e. an upstream low-frequency region, a transitional region and a downstream high-frequency region. The random-mode perturbation experiment also reveals that the spatial evolution of the spectral power of the peak frequency experiences two stages, firstly a decaying stage and secondly an amplifying stage downstream. Furthermore, the single-mode perturbation experiments present evidence for the occurrence of resonance of the thermal boundary layer subjected to perturbations at frequencies in the frequency band of resonance.

References

[1] Eckert ERG, Soehnghen E, Interferometric studies on the stability and transition to turbulence of a free-convection boundary layer, *Proc Gen Disc Heat Transfer*, 1951, 321-3.

[2] Hollman JP, Gartrell HE, Soehnghen EE, A study of free convection boundary layer oscillations and their effects on heat transfer, *ASME publication*, **60-SA-25**, 1960, 1-12.

[3] Polymeropoulos CE, Gebhart B, Incipient instability in free convection laminar boundary layers, *J Fluid Mech*, **30**, 1967, 225-39.

[4] Dring RP, Gebhart B, A theoretical investigation of disturbance amplification in external laminar natural convection, *J Fluid Mech*, **34**, 1968, 551-64.

[5] Gebhart B, Mahajan R, Characteristic disturbance frequency in vertical natural convection flow, *Intl J Heat Mass Transfer*, **18**, 1975, 1143-8.

[6] Gebhart B, Instability, Transition, and Turbulence in Buoyancy-Induced Flows, *Ann Rev Fluid Mech*, **5**, 1973, 213-46.

[7] Patterson JC, Imberger J, Unsteady natural convection in a rectangular cavity, *J Fluid Mech*, **100**, 1980, 65-86.

[8] Lin W, Armfield SW, Patterson JC, Unsteady natural convection boundary-layer flow of a linearly-stratified fluid with on an evenly heated semi-infinite vertical plate, *Intl J Heat Mass Transfer*, **51**, 2008, 327-43.

[9] Armfield S, Janssen R, A direct boundary-layer stability analysis of steady-state cavity convection flow, *Intl J Heat Fluid Flow*, **17**, 1996, 539-46.

[10] Patankar SV, Numerical Heat Transfer and Fluid Flow, *Hemisphere, New York*, 1980.

[11] Leonard BP, A stable and accurate convective modelling procedure based on quadratic upstream interpolation, *Computer Methods in Applied Mechanics and Engineering*, **19**, 1979, 59-98.